



Article

Continuous Detection of Surface-Mining Footprint in Copper Mine Using Google Earth Engine

Maoxin Zhang ^{1,*}, Tingting He ^{1,*}, Guangyu Li ², Wu Xiao ¹, Haipeng Song ¹, Debin Lu ¹ and Cifang Wu ¹

¹ Department of Land Management, Zhejiang University, Hangzhou 310058, China; 0619518@zju.edu.cn (M.Z.); xiaowu@zju.edu.cn (W.X.); shp0808@zju.edu.cn (H.S.); ludebin@zju.edu.cn (D.L.); wucifang@zju.edu.cn (C.W.)

² Institute of Land and Urban-Rural Development, Zhejiang University of Finance and Economics, Hangzhou 310058, China; guangyu@zufe.edu.cn

* Correspondence: tthe@zju.edu.cn

Abstract: Socioeconomic development is often dependent on the production of mining resources, but both opencast and underground mining harm vegetation and the eco-environment. Under the requirements of the construction for ecological civilization in China, more attention has been paid to the reclamation of mines and mining management. Thus, it is the basement of formulating policies related to mining management and implementing reclamation that detection of mining disturbance rapidly and accurately. This research carries on an empirical study in the Dexing copper mine, Jiangxi, China, aiming at exploring the process of distance and reclamation. Based on the dense time-series stack derived from the Landsat archive on Google Earth Engine (GEE), the disturbance of surface mining in the 1986–2020 period has been detected using the continuous change detection and classification (CCDC) algorithm. The results are that: (1) the overall accuracy of damage and recovery is 92% and 88%, respectively, and the Kappa coefficient is 85% and 84% respectively. This means that we obtained an ideal detection effect; (2) the surface-mining area was increasing from 1986–2020 in the Dexing copper mine, and the accumulation of mining damage is approximately 2865.96 ha with an annual area of 81.88 ha. We also found that the area was fluctuating with the increase. The detected natural restoration was appraised at a total of 544.95 ha in the 1988–2020 period with an average restoration of 16.03 ha. This means that it just restores less in general; (3) it has always been the case that the Dexing mine is damaged by mining and reclamation in the whole year (it is most frequently damaged month is July). All imageries in the mine are detected by the CCDC algorithm, and they are classified as four types by disturbing number in pixel scale (i.e., 0, 1, 2, more than 2 times). Based on that, we found that the only once disturbed pixels account for 64.75% of the whole disturbed pixels, which is the majority in the four classes; (4) this method provides an innovative perspective for obtaining the mining disturbed dynamic information timely and accurately and ensures that the time and number of surface mining disturbed areas are identified accurately. This method is also valuable in other applications including the detection of other similar regions.

Keywords: continuous change detection; google earth engine; Landsat; disturbance; vegetation; NDVI



Citation: Zhang, M.; He, T.; Li, G.; Xiao, W.; Song, H.; Lu, D.; Wu, C. Continuous Detection of Surface-Mining Footprint in Copper Mine Using Google Earth Engine. *Remote Sens.* **2021**, *13*, 4273. <https://doi.org/10.3390/rs13214273>

Academic Editors: Jordi Cristóbal Rosselló and Amin Beiranvand Pour

Received: 19 August 2021
Accepted: 21 October 2021
Published: 24 October 2021

Publisher's Note: MDPI stays neutral with regard to jurisdictional claims in published maps and institutional affiliations.



Copyright: © 2021 by the authors. Licensee MDPI, Basel, Switzerland. This article is an open access article distributed under the terms and conditions of the Creative Commons Attribution (CC BY) license (<https://creativecommons.org/licenses/by/4.0/>).

1. Introduction

In China, mineral output and its proportion have increased significantly. The non-ferrous metals (copper, aluminum, lead, and zinc) increased from 950,000 tons in 1978, accounting for 2.65% of the world's output, to 56.86 million tons in 2019, accounting for 50.27% of the total output in the world [1]. Mineral resources are indispensable to modern industrial raw materials. However, surface mining behaviors are able to directly damage the surface soil and vegetation [2]. Underground mining is likely to contribute to the collapse of land and then deteriorate the land and vegetation [3]. The extraction of non-ferrous metals usually consumes considerable energy and produces abundant wastes, which can result in the degeneration of the ecosystem and environmental problems [4].

Therefore, in order to realize the harmonious development of environmental protection and mine production, it is necessary to carry out effective protection and management.

Since the 1930s, the United States, Australia, Germany, and Canada have begun to attach importance to mine ecological restoration, and promulgated relevant laws and regulations, such as the Opencast Mining Management and Restoration (Reclamation) Act, which requires that “whoever destroys it, reclaims it”. Under the overall requirements of the construction in ecological civilization in China, great attention has also been paid to the governance of mines. China has enacted the Mineral Resources Law and the Standard for the Construction of Green Mines in Nonferrous Industries. In order to effectively implement the whole life cycle management of mining engineering, such as mining safety, prevention of geological disasters, ecological protection, and restoration, researchers and mining management agencies must continuously monitor the changes of strata and vegetation caused by man-made disturbances in mining areas. However, the traditional method of field investigation is unable to observe the previous mining history due to its time-sensitive characteristic, and the measurement data error may be caused by human behaviors, resulting in low efficiency with large consumption of human financial resources. In recent years, with the development of remote sensing platforms and sensors, continuous and repeated remote sensing observations of most areas in the earth’s surface have been achieved, and massive multi-source, multi-scale, and multi-resolution remote sensing data have been accumulated. Remote sensing monitoring has become an effective method for disturbance monitoring in mining fields.

The earliest application for remote-sensing monitoring is to compare the data of different years (that is, the comparison of multi-temporal classification results). This method usually directly uses the pixel spectral value, or the feature parameters such as vegetation index, texture feature, independent component extracted from the image, and then through principal component analysis (PCA) [5], change vector analysis (CVA) [6], pixel dichotomy model method [7], and decision tree [8], a direct comparison is made from those obtained difference image and extract the change information. A lot of practices have been carried out in mining areas, including vegetation degradation and reclamation [9], land use cover and change monitoring in mining areas [4,10], ecological landscape monitoring in mines [11,12], and vegetation change monitoring in mining fields [13]. The comparison of temporal classification results is the basic method of change detection, which is suitable for imageries processing and analyzing with fewer temporal phases. The technical key could be contributed to the construction of change detection index and the determination of change threshold, generally, which is an interval of 2 years, 5 years or even 10 years. However, the interval is still insufficient compared with the growing demand for the analysis of long-time sequence and mass remote sensing imageries.

With the accumulation of a large number of historical data in the same region and different periods, the high time-resolution remote sensing data can be easily obtained. As a result, the change detection of remote sensing time series imageries has been popular in remote sensing technology and application in recent years. The time-series analysis usually uses single-band quantitative parameters (such as NDVI) as input data instead of multi-spectral images and uses simultaneous phase such as monthly or season time-series images over the years to effectively explore the time-series change information of ground features. The method of combining multi-temporal remote sensing images with time series analysis can effectively record and analyze the characteristics of land use cover and changes in the spatio-temporal range [14]. The combined method has been applied broadly to the detection of ground disturbance in the mining area. For instance, based on typical disturbance trajectories of coal mining subsidence area derived from those multi-temporal remote sensing imageries, Wang et al. (2019) applied the decision tree algorithm to identify the process characteristics of coal mining and its disturbance on surface vegetation in the past 34 years [15]. Li Jing et al. (2016) downloaded 22 items of Landsat TM/ETM+ multispectral images of the Weizi County coalfield, Appalachian region [16]. Through the remote sensing time series analysis method of combining forest

characteristic index and normalized vegetation index, it was found that there were ecological dynamic characteristics of land-use/cover change (LUCC) in this area in the past 27 years. At the same time, massive remote sensing data has promoted the development of change detection algorithms, including VCT, BFAST, LandTrendr, CCDC etc., which are widely used in the disaster, forestry, land and other research fields. Huang et al. (2010) use the highly-automated vegetation change tracker (VCT) algorithm and Landsat time series stack (LTSS) to reconstruct the recent history of forest disturbance [17]. The break detection for additive and trend (BFAST) method based on breakpoint detection is commonly used in the information detection of NDVI and EVI from remote-sensing imageries such as MODIS and Landsat [18]. Kong et al. (2015) used the empirical mode decomposition (EMD) method to extract trend terms and seasonal terms of NDVI time series for forest fire detection [19]. The LandTrendr algorithm proposed by Kennedy takes the year as the time interval, and collects the Landsat time-series data of similar time every year for time segmentation to obtain the disturbance information of forest vegetation [20]. Zhu and Woodcock proposed the CCDC model, which has been widely applied in the field of remote sensing image time series change detection, such as land change monitoring and assessment [21], urban expansion change information extraction [22], and forest disturbance information extraction [23].

In recent years, Google Earth Engine (GEE) has collected commonly used remote-sensing data sets such as MODIS, Landsat, and Sentinel [24] and can obtain and process shared data by programming online or offline. Cloud computing analyzes and processes remote-sensing data, which avoids the tedious process of data download and preprocessing compared to the traditional remote sensing analysis model. This also contributes to the development of the time change detection algorithm significantly. LandTrendr, CCDC and other algorithms are also integrated on the Google Earth Engine platform to quickly access applications [25] which are widely used in the change detection such as disturbance and restoration of woodland [26], wetland land cover type [27], urban expansion [28], subsidence water in coalfield [29], and disturbances in the mining area [30]. Among those algorithms, the CCDC algorithm has advantages such as automatic processing, high universality, less data limitation, and avoiding the accumulation of classification errors compared with other methods. At present, the CCDC algorithm, however, has not been applied to disturbance detection in the mining area. Therefore, based on the GEE platform, this study intends to select the largest copper mine in Asia as the research object, and apply all available Landsat time series with the CCDC algorithm to detect the surface disturbance process of the mining area.

The purpose of this study are as follows: (1) based on highly dense remote sensing data, the CCDC algorithm is used to detect the disturbance time caused by mining in Dexing Copper Mine, and to detect and analyze the spatio-temporal characteristics of open-pit mining; (2) then, we verify the accuracy of the CCDC algorithm in detecting surface disturbances in the mining area; finally, (3) we validate the effectiveness of the CCDC algorithm in detecting mining footprints through multiple case studies and multiple methods comparison. Two questions are considered in this study: (1) how many the area of land damaged and reclamation in Dexing copper mine from 1986 to 2020; (2) Can Landsat NDVI time series be combined with the CCDC algorithm for detection of surface-mining footprint?

2. Materials and Methodology

2.1. Study Area

The Dexing Copper Mine is located in the middle and lower reaches of the Yangtze River, located in Dexing country, Shangrao city, northeast of Jiangxi province ($117^{\circ}43'40''$ E, $29^{\circ}01'26''$ N) (Figure 1). It belongs to the Huaiyu Mountains with the neighboring Damao Mountain. The mining area includes industrial sites and living areas such as mining, separating, and auxiliary facilities. The copper mine belongs to the middle and lower hilly area, which is high in the southeast and low in the northwest, and its river system

is well developed. The Lean River located in the north of the mining area is the main source of domestic water in the mining region, while the Dexing River located in the south is for Dexing City and its lower reaches. The rest of two rivers are Dawu River to the west and Fujiawu River to the east. The average annual temperature in the study area is 17.3 °C. The average temperature in January can reach 5.6 °C, and the minimum temperature is as low as −8.9 °C, while the average temperature in July is 29 °C and the highest is 42 °C. The average annual precipitation is 1981 mm. Since the vegetation will grow luxuriantly in which abundant rainfall has, consequently, the bedrock of the study area is weathered seriously and the outcrop is very poor. Dexing Copper Orefield is composed of those three ore deposits (i.e., copper factory, Fujiawu and cinnabar) and is the largest open-pit copper mine in Asia with the first annual output in China. At present, more than 20 kinds of mineral deposits such as gold, silver, copper, manganese, zinc, phosphorus, dock, and iron have been proved, of which the reserves of Au and Cu have reached 580 t and 5000 t, respectively. There are two main reasons why we chose Dexing Copper Mine as the study area. One is the large scale of Dexing Copper Mine, which has been exploited for hundreds of years and needs to be exploited continuously in the future. This change and dynamic geographical environment provide a valuable opportunity to test our method. Second, the climatic conditions in this area are beneficial to the growth of vegetation and high vegetation coverage. However, surface stripping and waste rock dumping in mining directly damage the original vegetation on the surface. The detection of vegetation in mining areas is a direct method to test the effect of reclamation and environmental governance.

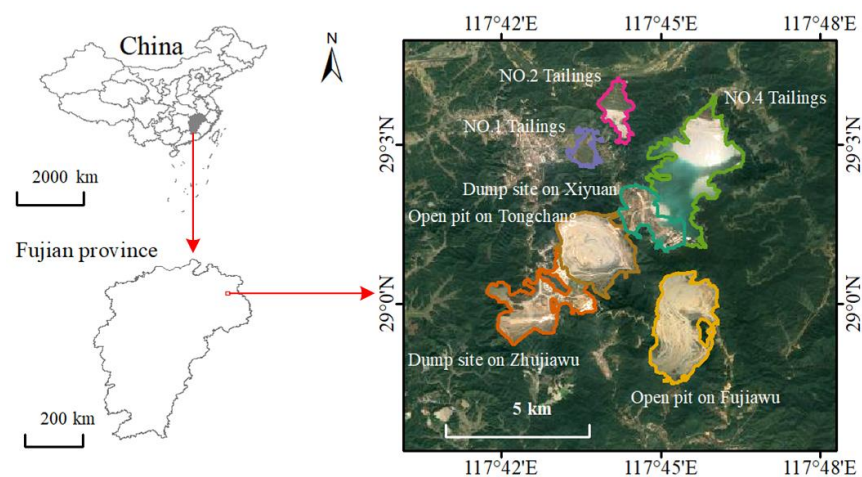


Figure 1. Study area (the geographic data from Yu et al. (2009) [31]).

2.2. Overview

Opencast mining has led to the direct damage of surface vegetation, so the mining process can be characterized by the change of vegetation. The time series tracks of vegetation index in the mining area include the following six types: (1) the vegetation has not been damaged and the vegetation index has been at a high value (Figure 2a-①); (2) the vegetation has been damaged before the study period and has not been reclaimed in the later period (Figure 2a-②); (3) the vegetation has been damaged before the study period and reclaimed in later stage (Figure 2b-③); (4) the vegetation is not reclaimed after damage, and the vegetation index is finally at a low value (Figure 2b-④); (5) the vegetation is reclaimed after damage, and the surface is finally covered with vegetation (Figure 2c-⑤); and (6) the surface vegetation undergoes the process of multiple damage and restoration (Figure 2d-⑥). It is obvious that there is an obvious sudden change signal in the process of vegetation damage and reclamation, so the breakpoint information in the trajectory can be found by time-series change detection. Finally, the footprint information of the mining area is obtained, including disturbed time and times.

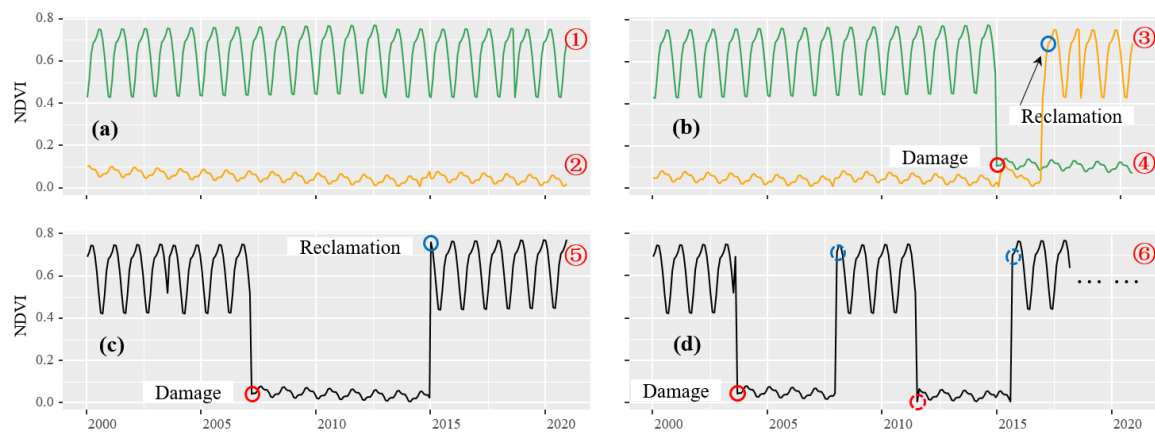


Figure 2. Six types of NDVI trajectory. (a) Undamaged vegetation① and persistent bare land②; (b) damaged vegetation before the study period, reclaimed later③ and damaged vegetation④; (c) reclamation vegetation after damage⑤; (d) repeatedly disturbed mining areas⑥.

The technical process of this study is shown in Figure 3, which includes three parts: (i) data preprocessing; (ii) damage and reclamation detection of vegetation in surface mining areas; and (iii) accuracy verification. First, the Landsat surface reflection data are preprocessed by masking snow and cloud cover, and the time-series remote sensing data from 1986 to 2020 are obtained, which is used to calculate NDVI. Then, the CCDC algorithm is used to detect the disturbance spatio-temporal information from the NDVI trajectory. The disturbance information includes the damage time and the reclamation time, and identifies type of disturbance base on the occurrence pattern of disturbance events. Finally, combined with Google Earth, sample points are selected to verify the accuracy.

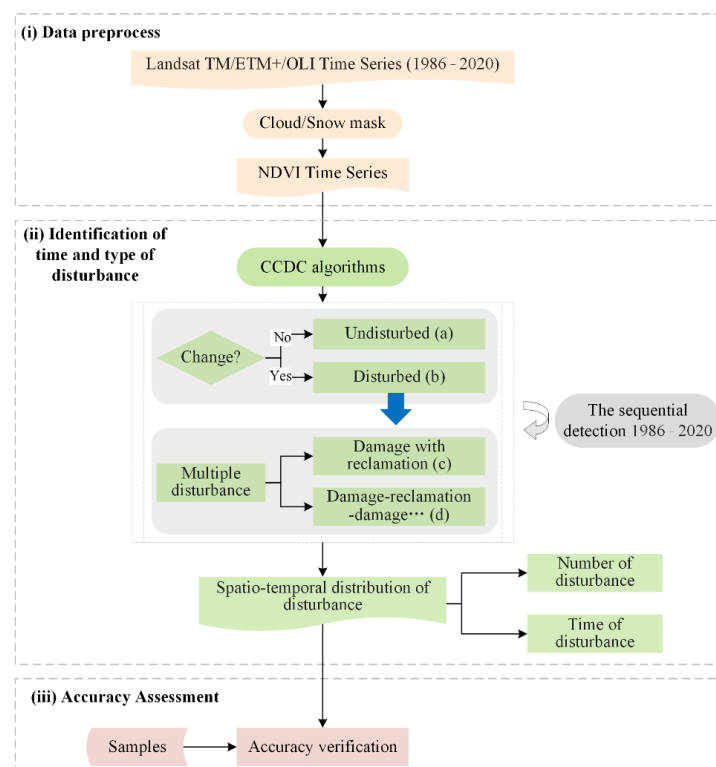


Figure 3. Workflow of the methodology.

2.3. Satellite Data and Image Preprocessing

The Google Earth Engine (GEE) platform is a cloud-based geospatial analysis platform that provides access to USGS level 1 and level 2 Landsat data (<https://espa.cr.usgs.gov/>, accessed on 23 October 2021) with enormous computing power [24]. Through GEE, all available Landsat TM/ETM+/OLI imageries are obtained easily, which are Landsat/LT05/C01/T1_SR, Landsat/LE07/C01/T1_SR and Landsat/LC08/C01/T1_SR respectively. Based on the study area and research time (1986–2020), we obtained geometrically and atmospherically corrected (i.e., USGS Level 1T) Landsat 4 and 5 thematic mapper (TM), Landsat 7 enhanced thematic mapper (ETM+) and Landsat 8 operational land imager (OLI) data, including 685 imageries from the US Geological Survey-Earth Resources observation and Science online Portal for all cloud cover areas with less than 80% cloud cover [24,32].

2.4. Surface Disturbed Processes and CCDC Algorithm

Mining activities include the removal of surface cover and the dumping of cover, which may result in a sudden transformation of the natural environment into bare land or buildings. This study is based on the premise that surface mining and reclamation will cause sudden change of vegetation, and the track of vegetation index can be used to detect the change. Karan et al. (2016) show that NDVI is the best index to detect the change of coal mine vegetation [33]. The NDVI formula is as follows:

$$NDVI = \frac{\rho_{NIR} - \rho_{red}}{\rho_{NIR} + \rho_{red}}$$

where ρ_{NIR} and ρ_{red} represent the reflectivity of ground objects in near-infrared red band and red band, respectively. The typical time series track of vegetation in the study area includes three states, namely vegetation cover before damage, bare land formed after damage, and vegetation cover after reclamation. Time series analysis is used to find breakpoints in the trajectory to indicate sudden changes. As shown in Figure 4, in the process of surface mining the soil and rock covering the deposit are removed and the vegetation is damaged. In the process of removing the cover, stripping and dumping will destroy a large amount of vegetation. The NDVI index decreased significantly in 1996, and the damaged time was set to 2 February 1996. Subsequently, the dump in this area was recycled and the vegetation was gradually restored. The NDVI index rose in 2016, and the reclaimed time was set at 1 December 2016.

Continuous land cover change detection and classification algorithm (CCDC) is a time series method proposed by Dr. Zhu of the University of Connecticut in 2014. This algorithm is different from traditional methods and is mainly based on Landsat time series with less noise. It is an “online” algorithm for each pixel, and clouds and cloud shadows can be filtered through CFmask (from QA band) and multi-temporal mask (Tmask) algorithm. When new satellite data are obtained, the CCDC algorithm combines all available Landsat observations for each pixel to estimate time series models, which can be used to predict future observations. If the new continuous observations exceed the expected range, a breakpoint is marked and a new time series model is estimated (two time series segments will be generated before and after the change, otherwise only one period will be generated for stable pixels). Until the next breakpoint is detected or the observations are exhausted, all breakpoint signals in the middle and inter-annual of the trajectory data are finally identified. Breakpoints can be figured out in the time series of data, such as those mutations caused by land cover changes. By calculating the number of breaks per pixel, we can get a map of the total number of changes. On the other hand, by recording the spectral change amplitude of the detected breakpoint, we can distinguish the conversion type of land use. Besides, the happening time of those points which has been recorded, we can provide the time of land cover change.

Mining activities, including surface stripping and waste rock disposal, directly lead to the damage of surface vegetation. CCDC algorithm can be used to detect vegetation damage and restoration caused by mining. We collected 200 sample sites by Google Earth

TM, and proved that the CCDC algorithm and NDVI index can effectively distinguish and identify vegetation and bare land. Figure 4 shows the difference between vegetation and bare land in the NDVI fragment segment.

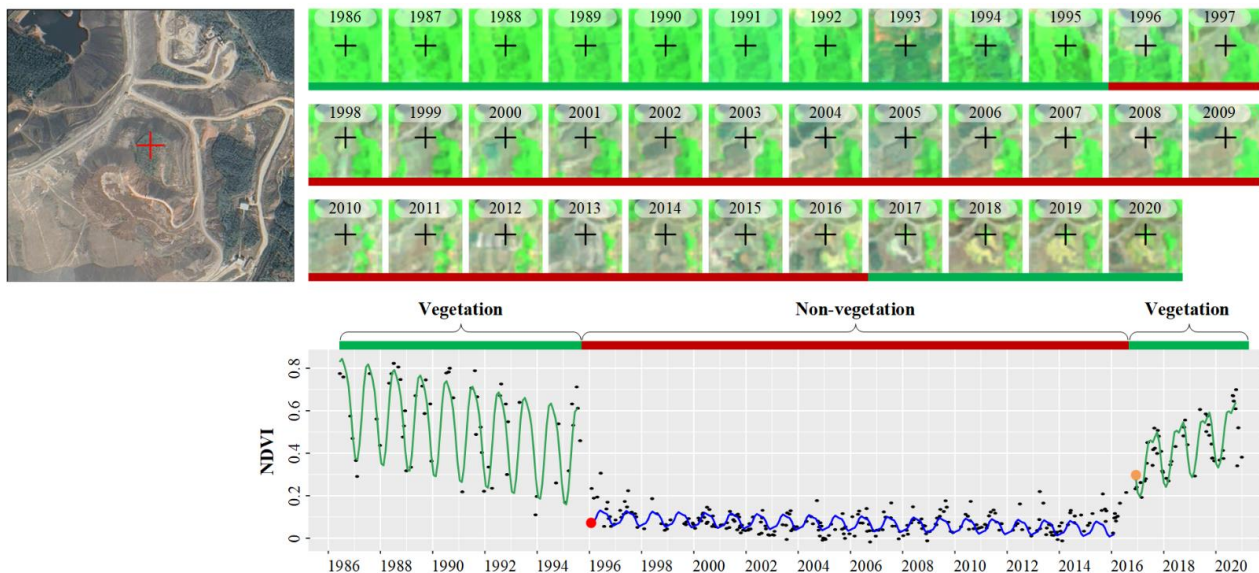


Figure 4. Trajectory data and corresponding images false color composite image (SWIR2/NIR/Green). The cross shape is the location of the sample point; the black point is the original NDVI value; the green line is the fitted vegetation track; the blue line is the fitted bare ground track; the red point is the breakpoint of vegetation damaged; and the orange point is the breakpoint of vegetation reclamation.

2.5. Identification of Damage and Reclamation Spatio-Temporal Processing

In the process of mining, the surface is stripped or covered by slag, resulting in a sharp decline in vegetation coverage. First of all, we fit and segment the NDVI trajectory to get the NDVI segmentation by the CCDC algorithm. Then the disturbance pixels of vegetation are extracted by the change amplitude of NDVI fragments. Reference He et al. (2020) [29] the method for determining the threshold, we choose 100 damage (60 reclamation) sample points and the parameter in $[0.2, 0.6]$ ($[-0.2, -0.6]$) by the interval of 0.05 to calculate the accuracy of detecting damage (reclamation). Finally, we choose the decrease (increase) of NDVI by 0.3 (0.25) as the optimal threshold to determine damage (reclamation). For multiple-segmented pixels, the minimum of multiple damage time is set as the final damage time, while the maximum of multiple reclamation time is set as the final reclamation time. Importantly, the end of the trajectory must be an ascending segment. As a result, the damaged and reclaimed time mapping of the area is completed. To reduce the noise in the patches of damaged time, the damaged time of the adjacent pixels is mostly continuous. Therefore, we smooth the damaged-time patches by mode algorithm. It is worth noting that, for the pixels that have been damaged before 1986 and have not been reclaimed during the study period, we set the damaged time of these to 1 January 1986.

2.6. Validation

Considering the difficulty to obtain public remote-sensing data with a high time-and-spatial resolution, we verify the accuracy of abrupt change time per year. Fifty points per year are randomly selected in the damaged area, while twenty points per year are selected in the reclamation area. The detection time of damage year is from 1986 to 2020, and that of reclamation year is from 1988 to 2020. 1750 damage samples and 660 reclamation samples were detected. Then, the high-resolution image data on Google Earth are used for interactive visual calibration to determine the damage year and recovery year of each sampling point. By comparing the sample label with the recognition results of the algorithm,

the user accuracy, producer accuracy, overall accuracy, and kappa coefficient of mining damage and reclamation detection are calculated, and the change detection and accuracy are verified.

3. Results

3.1. Accuracy

The overall accuracy of damage and recovery is 92% and 88% respectively, while the kappa coefficients are 85% and 84% respectively (Figure 5). Although the overall accuracy of a given year is high, the accuracy of producers and users in damage accuracy detection is mainly between 82% and 95%, and that of producers and users in recovery accuracy detection is mainly between 75% and 92%. In some specific years, the accuracy of year recognition is relatively lower. For example, in the recovery accuracy test, both user accuracy and producer accuracy were less than 75% in 2005, which may be due to the incompetent quality of remote sensing data in these years.

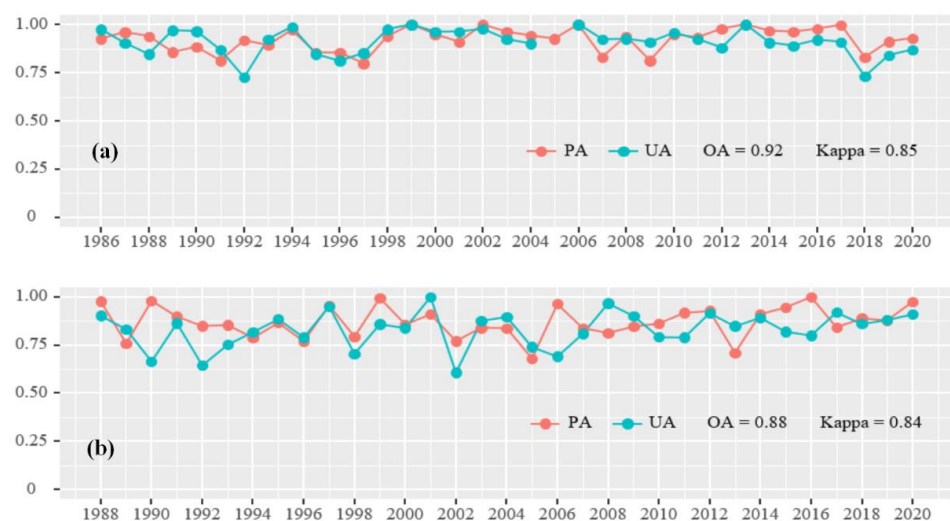


Figure 5. Accuracy verification of damaged year and restored year. (a) Accuracy of the damaged year; (b) accuracy of the restored year. PA: producer's accuracy; UA: user's accuracy; OA: overall accuracy.

3.2. Spatio-Temporal Characteristics of Surface Disturbance

The damage detection in the mining area lasted for 35 years from 1986 to 2020 (Figure 6a,c), and the surface damage area in the region continued to increase, with a cumulative damage area of 2865.96 ha and an average annual damage area of 81.88 ha. Among this damages, there are 17 years wherein the intensity is higher than the average level. The biggest damage in the area occurred in 1986, covering an area of 292.68 ha. What causes the intensive degree is that Dexing copper mine was established in 1958, Beishan Mine was built in 1965 for underground mining, and Nanshan Mine was built in 1971 for opencast mining. The result of 1986 identification is the cumulative value of the damage area in 1986 and before. Additionally, the largest damage area was happened in 1992, reaching 147.06 ha. From the perspective of damage distribution, before 1986, the damage area was mainly distributed in No. 1 tailings reservoir, No. 2 tailings reservoir and Tongchang mining area; and after 1990, the damage area first moved north to the location of No. 4 tailings reservoir, and then turned to Zhujia dump site in the southwest, which caused by mining outward from the center with time. After 2004, the mining core area was transferred to the Fujiawu mining area in the southeast.

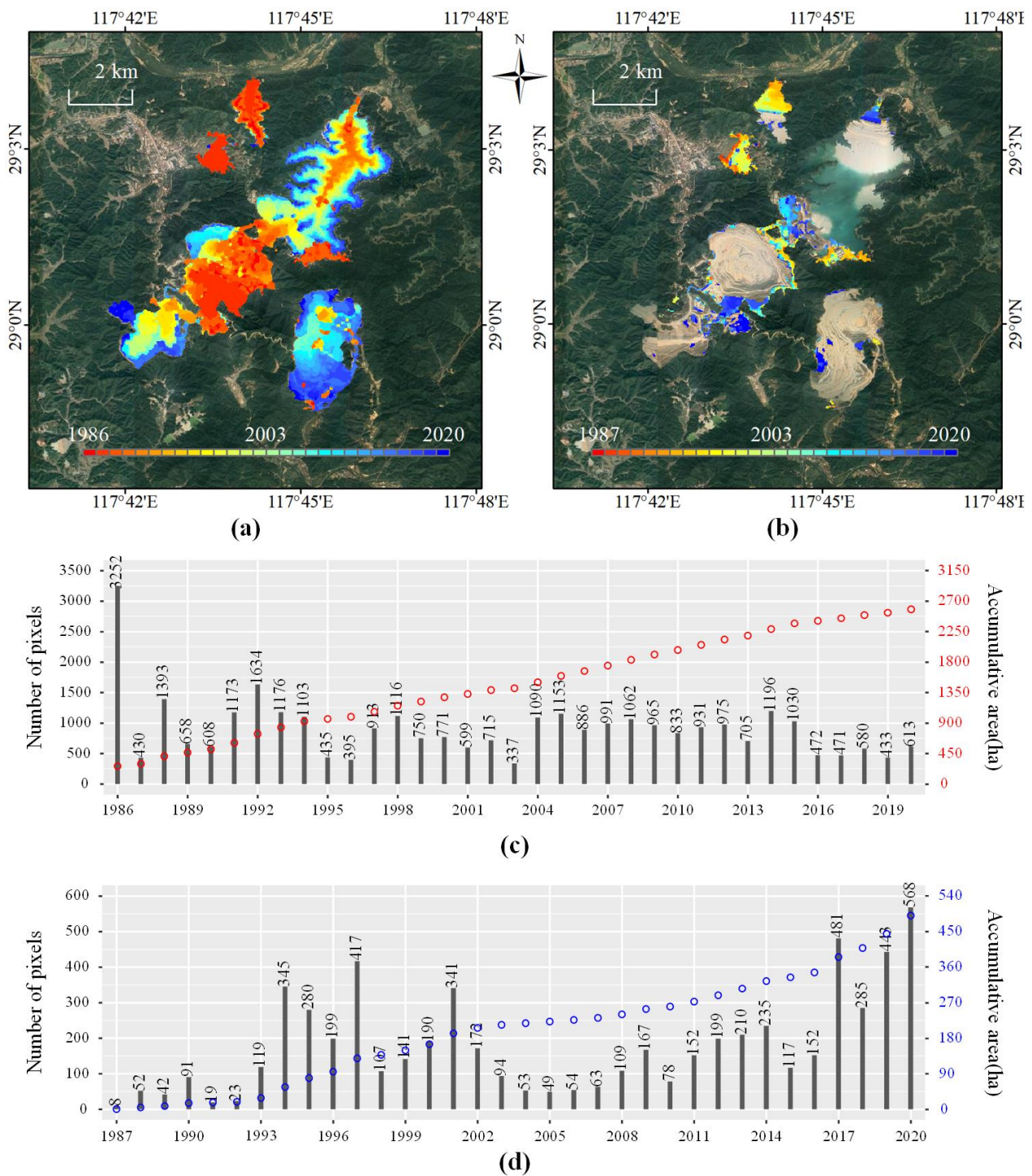


Figure 6. Map of damage year (a) and reclamation year (b); statistical diagram of the damage area (c) and the reclamation area (d).

Natural restoration and reclamation detection in the mining area had been 34 years from 1987 to 2020 (Figure 6b,d), and the total restoration area is 544.95 ha with an average annual recovery of 16.03 ha. There are 12 years in which the vegetation restoration area is higher than the average, and the maximum value is 51.66 ha in 2020. The total area of natural or artificial restoration is gradually increasing, mainly from 1994 to 1997, 2001, and 2017 to 2020. From the distribution of ecological restoration in Dexing mining area, from 1994 to 1997 and 2001, it was mainly concentrated in No. 1 tailing reservoir, No. 2

tailing reservoir, and scattered in Xiyuan dump site. From 2017 to 2020, the intensity of vegetation restoration increased obviously, and the north of No. 4 tailing reservoir, Zhujia dump site, Fujiawu mining area and the area scattered in Xiyuan dump site were concentratedly restored.

We further investigated the year of damage and reclamation for each pixel and counted the number of pixels in a three-year cycle. The results are shown in Table 1, in which the horizontal row represents the year of reclamation and the vertical column represents the year of destruction. The results show that the number of pixels of land damaged in the 1986–1988 period was 5075, of which 55.8% of pixels were reclaimed. The earlier the land was damaged, the higher the probability of restoration. After 2004, the vegetation reclamation rate of damaged land was less than 10%.

Table 1. Transfer matrix of damage years and reclamation years for pixels. Horizontal is the damage year, vertical is the reclamation year.

	T1	T2	T3	T4	T5	T6	T7	T8	T9	T10	T11	T12	Total	RR
T1 = [1986, 1988]	50	142	364	612	293	375	91	137	80	91	357	243	5075	0.558
T2 = [1989, 1991]		3	105	153	42	112	17	52	22	38	45	189	2439	0.318
T3 = [1992, 1994]		4	7	107	91	72	21	62	86	127	186	129	3913	0.227
T4 = [1995, 1997]		2		2	5	14	7	17	9	18	57	67	1743	0.113
T5 = [1998, 2000]				3	5	19	8	27	47	50	37	16	2637	0.080
T6 = [2001, 2003]			1	1	1	1	3	17	117	68	26	29	1651	0.159
T7 = [2004, 2006]			4	8	1	7	8	17	16	71	36	93	3129	0.083
T8 = [2007, 2009]	2			1				2	40	28	78	98	3018	0.082
T9 = [2010, 2012]				8		6			6	65	67	74	2739	0.082
T10 = [2013, 2015]							1	8	6	1	29	56	2931	0.034
T11 = [2016, 2018]			5	1		1				3		17	1523	0.017
T12 = [2019, 2020]		1	1							2		0	1046	0.003

Note: RR indicates the ratio of pixels that reclaim in a period.

3.3. Months and Times of Surface Disturbance

The surface disturbance (damage and restoration) in the Dexing mining area will occur throughout the year (Figure 7). The mining in each month is higher than 1500 detection pixels, and the highest amount appears in July which is more than 3500 pixels, while the followed highest amount months are March and September. The mining disturbance is less in January, February, October, and December, mainly due to the cold that cause seasonally freeze of some soil layers in winter. In terms of vegetation restoration, the restored number of pixels in July is the highest, which is more than 500 pixels, and the lowest amount is in January, which is less than 200 pixels. Most restoration occurs in the months with high temperatures from March to September, which is beneficial to the growth of vegetation.

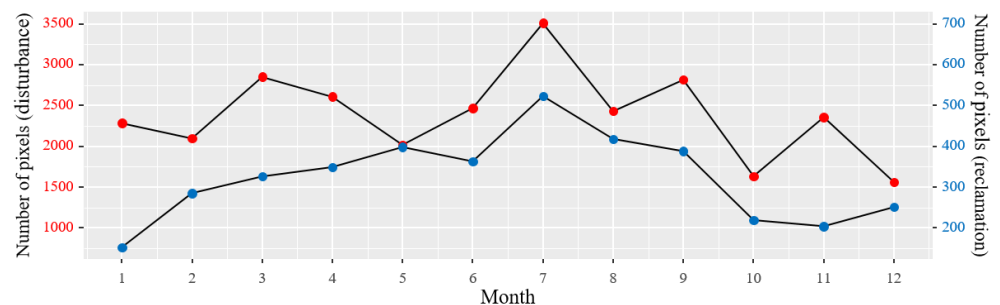


Figure 7. Statistical chart of damaged months and recovery months.

The CCDC algorithm detects all the imageries in the mining area. It also identifies four types that represented the number of pixel disturbances which are 0, 1, 2, and more than 2 times (Figure 8), respectively. Type “0” was mined before 1986 and it accounts for 4.24% of the disturbed pixels. Type “1” are able to contribute that the first disturbance may be mining, or it may be the case of recovery after disturbance before 1986. Type “1” has the largest number of pixels in disturbance, accounting for 64.75% of the total. Type “2” represents two disturbances, that is reclamation after mining, or mining after reclamation. The pixels of this type account for 24.71%. Type “3” means that there had been happened three times repeated disturbances, which accounts for 6.30% of the disturbed pixels. From the perspective of geographical distribution, Type “0” is mainly distributed in the opencast mine of the Tongchang mining area, indicating that the mining was carried out before 1986, and the vegetation has not changed since then. The area of Type “1” is widely distributed. It is worth noticing that most of the area of No. 1 and No. 2 tailings reservoirs had been disturbed once, but it appears in the above results of surface vegetation restoration. The reason is that a larger proportion of No. 1 and No. 2 tailings reservoirs had been mined before 1986. Type “2” are distributed in the areas such as No. 2 tailing reservoir and No. 4 tailing reservoir, which is basically consistent with the results of vegetation restoration mentioned above, indicating that these areas are mined and restored after 1986. The disturbances of more than 2 times are concentrated in the Xiyuan dump site where it has experienced repeated surface disturbances.

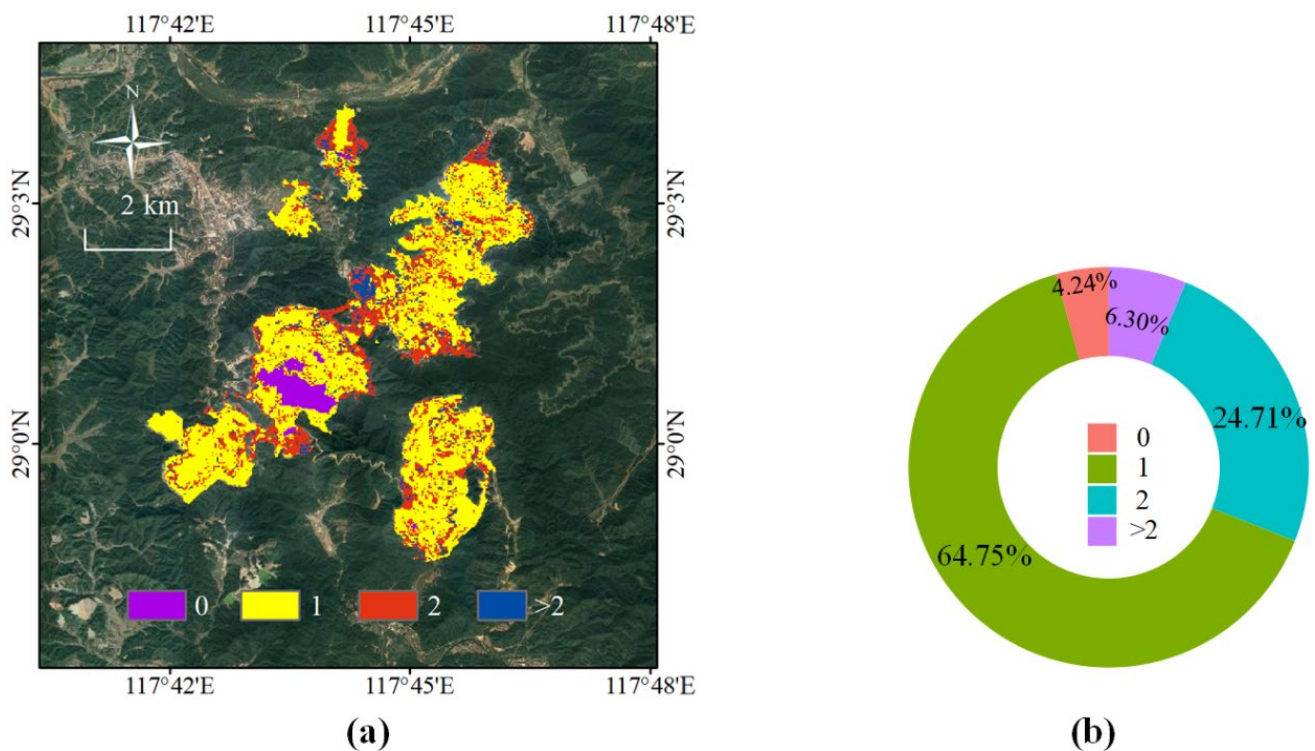


Figure 8. (a) Map of disturbance frequency and (b) statistical graph of disturbance times.

4. Discussion

4.1. Continuous Change Detection Using Landsat Time-Series Datasets

The mining in Dexing mine involves the safety of resources and environment, which is widely concerned by academia. Many scholars use EO-1, Hyperion, GeoEye-1, and other remote sensing data to monitor the mining circumstance in the Dexing copper mine [31,34,35]. However, the existing methods for the study of the location are based on fewer images and long-time-interval, thus the downloading is such consuming of time and labor. The continuous mining process of the Dexing copper mine cannot be detected by those methods, which contributes to delays and limitations for the detection in subsequent

vegetation restoration. There are nearly 40 years of data archiving history for Landsat data, which has a high spatial resolution, good consistency and free and open policy [36]. After the change of vegetation coverage, it can be found that NDVI value changes obviously. Landsat time series of NDVI has been successfully used in plenty of researches, including forest degradation [37], urban expansion [28] and abandonment of cultivated land [38]. Those advantages make it play an important role in the earth observation system and promote the development of efficient change detection algorithms based on time-series trajectory data. In this paper, the change detection of surface damage and reclamation in the opencast mining area is carried out based on Landsat TM/ETM+/OLI time-series stacks data. The results show that the CCDC algorithm can detect the annual variation of surface disturbance in the mining area. This continuous change detection is redounded to improve the coarser time information extracted due to the insufficient time density of the data.

4.2. Multi-Segment Segmentation and Sensitivity Analysis

The mining-disturbed detection based on GEE and CCDC algorithm has been proved that it is higher sensitive than other methods. For example, some scholars detect land damage and reclamation in surface coalfield based on the GEE and LandTrendr algorithms [26]. Based on annual data and Landsat sequence data, the algorithm constructs a long-term track of annual pixels and then generates an annual NDVI index to represent the annual change of pixels. In a different manner, the CCDC algorithm combines all of the available time series of Landsat observation data in each pixel to identify the damaged or restored pixels according to the trajectory of the vegetation index. This method avoids the error caused by the superposed annual data. In this research, 685 imageries were detected by the CCDC algorithm from 1986 to 2020, instead of 35 images detected by LandTrendr. CCDC also has the advantage that its pixel disturbed detection can be accurate to months and times, which can identify mining disturbance more accurately and sensitively. The method is helpful to grasp the situation of mining and reclamation timely, which is conducive to dealing with geological disasters and implementing ecological environment monitoring.

4.3. Adaptability Analysis of CCDC Algorithm in Mining Footprint

In order to analyze the universality of CCDC algorithm in detecting mining footprint in open-pit mining area. We randomly select three counterpart areas in Ukraine, India, and Australia, and detect the mining footprint of them using CCDC algorithm. Figure 9 (the first row) shows the location of those three areas, and Figure 9 (the third row), respectively, shows the result of inter-annual footprint of mining. The overall accuracy of the three mining areas is 91% (Ukraine), 83% (India), and 87% (Australia), respectively, in addition to the kappa coefficients corresponding to 90%, 82%, and 85%. The CCDC algorithm can be easily available to the detection of mining footprints in different mining areas. The reason is that mining activities have led to obvious changes in surface vegetation. Based on the variation range of NDVI and CCDC algorithm, it has been successfully applied to mangrove long time sequence mapping [39], grassland fire detection [40], and urban greenness trend analysis [41].

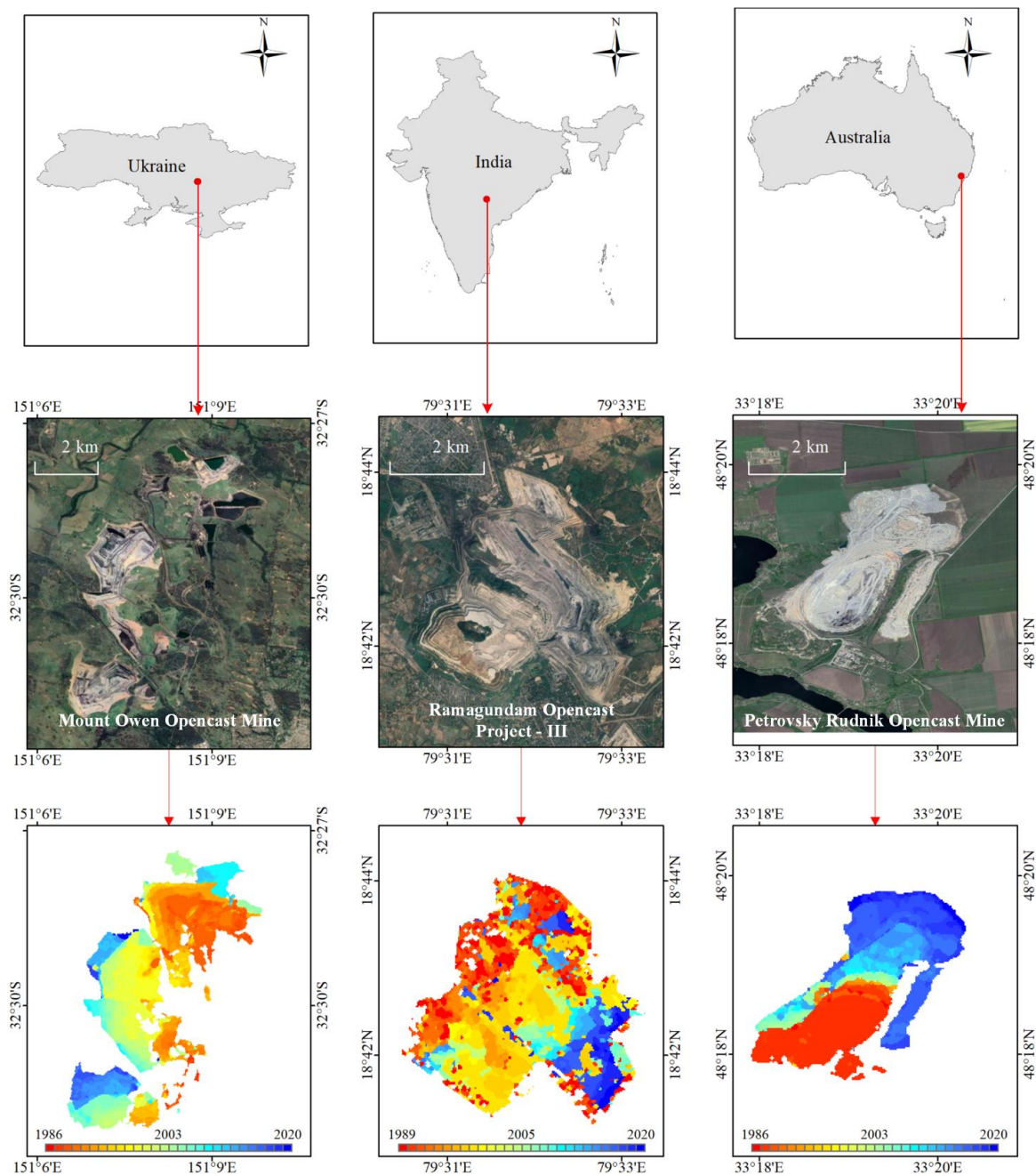


Figure 9. Open pit areas and corresponding mapping of damage year. The first row is the relative position of the mine site; the second row is a high-resolution map of the mining area from google earth; the third row shows the damage year map of the open pit areas from 1986 to 2020.

4.4. Comparison with Existing Methods

Yang et al. (2018) used LandTrendr algorithm and Landsat time series data to detect the surface disturbance process of coal mine [26]. Barenblitt et al. (2021) have studied the gold mining footprint, based on the trajectory of the annual maximum NDVI, and the maximum derivative method [42]. LandTrendr is a set of spectral time segmentation algorithm, which can be used to detect the change of time series of medium resolution satellite images [43]. The maximum derivative method (MaxSlope) uses the maximum change rate of NDVI to identify the occurrence of the maximum NDVI loss, which representing the type change from vegetation to mining [42]. We compare the results of this study with those data, including the maximum NDVI time series, the detected mining footprint in the study area

by the LandTrendr algorithm, and the maximum derivative method. Figure 10 shows the accuracy comparison of LandTrendr, MaxSlope and CCDC algorithm. Among the user accuracy (UA), the accuracy of LandTrendr algorithm fluctuates the most, and the user accuracy and producer accuracy (PA) of LandTrendr are generally lower among those algorithms. The reducing order of overall precision is CCDC, MaxSlope and LandTrendr. The difference between CCDC algorithm and the rest of algorithms might be determined as the model hypothesis. LandTrendr uses the inter-annual NDVI loss threshold to determine the transition year, MaxSlope using the year with the highest inter-annual NDVI loss rate as it. However, CCDC identifies the NDVI loss threshold in the vegetation growth cycle to determine the converted time [44].

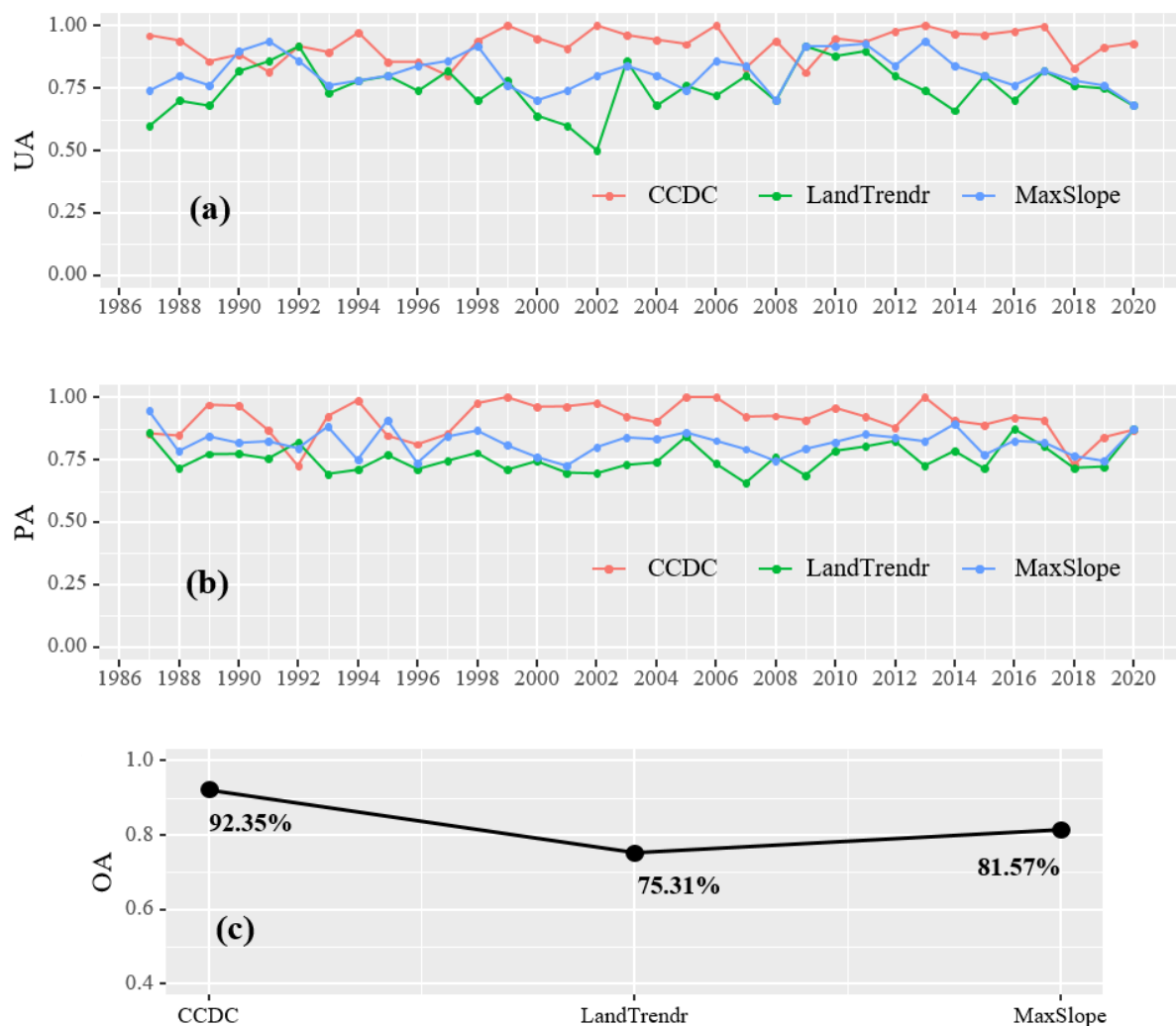


Figure 10. Accuracy of the damage year identified by the CCDC, LandTrendr and MaxSlope algorithms. (a) User's accuracy (UA) of the damage year; (b) Producer's accuracy (PA) of the damage year; (c) Overall accuracy (OA) of the damage year.

4.5. Comparison with Existing Products

Among the present global land cover products, GlobeLand30 products is full-factor surface cover products in high spatial resolution (30 m), including the data of 2000, 2010, and 2020. Due to the high quality, the products have been applied in many research fields [45]. In this study, we select the rectangular of 3 km × 3 km, the southwest of Zhujia dump site, and the data of 2010 and 2020, which are used to identify and compare the mining-damaged results by GlobeLand30 products and CCDC algorithm, respectively. In addition, we choose the national land cover dataset (NLCD, 30 m, available year: 2010, 2015, 2018) [46], annual China Land Cover Dataset (CLCD, 30 m, available year: 1990–2019) [47]

and MODIS Land Cover (MLC, 500m, available year: 2001–2019) [48]. Considering the time consistency of data products, we selected two periods of data in 2010 and 2018 to further compare the differences between the product data and this study results. The results show that the CCDC algorithm and CLCD products can accurately identify the surface damage in the northwest (Figure 11 the black circle), but the GlobeLand30 products and NLCD products are unable to identify it in the south (Figure 9 the yellow circle). The main reason is that GlobeLand30 products classify land use based on the time nodes of remote sensing data, wherein it is easy to lose inflection point information and form cumulative errors [49]. However, the CCDC algorithm is based on the change detection results of continuous NDVI trajectories. What we detected based on it has contained the complete catastrophe information from 2010 to 2018 and from 2010 to 2020. The CLCD products and MLC products are annual continuous products. CLCD products combine the post-processing methods of spatial-temporal filtering and logical reasoning, to improve the spatial-temporal consistency of annual products, and the results of change detection are relatively consistent with those of CCDC algorithm [47]. MLC products have a low resolution (500 m), which is difficult to accurately detect the surface disturbance information in mine. Above all, the vegetation-damaged boundary identified is closer to the surface soil mining stripping boundary in the original image. Therefore, the vegetation disturbance detection method proposed in this paper is better than the traditional comparison method.

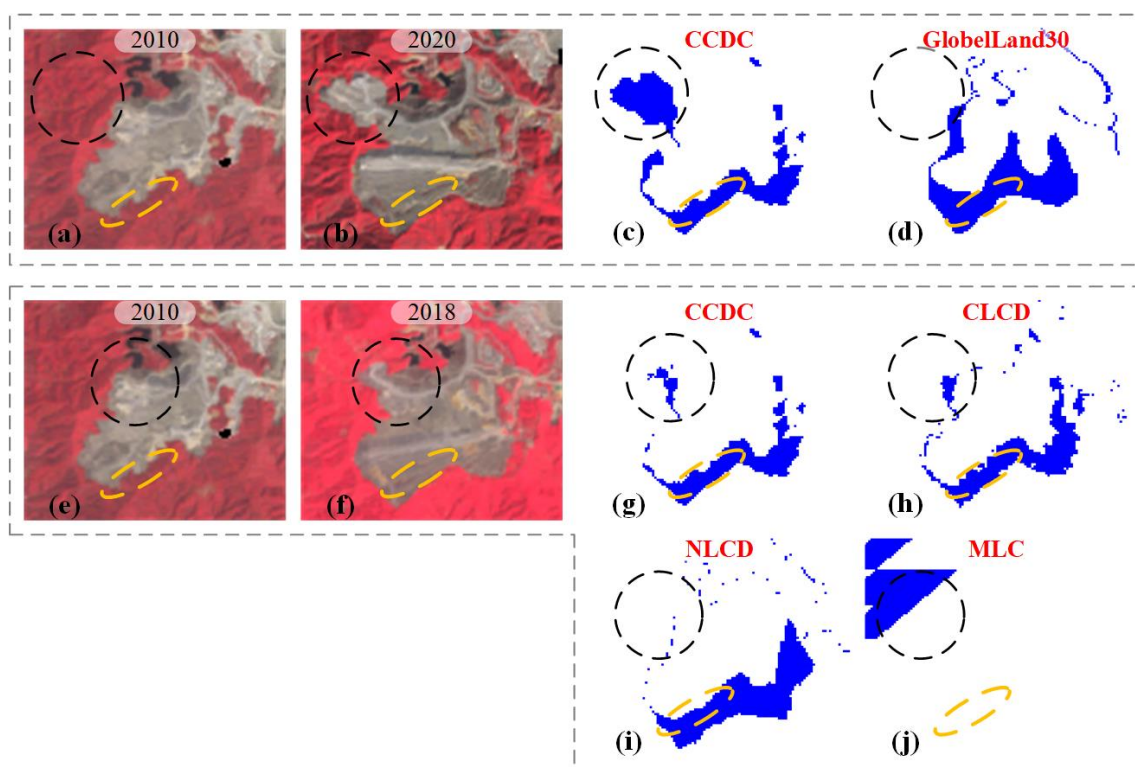


Figure 11. The typical area is the vegetation damage area during the period of 2010–2020 (2010–2018). (a,b,e,f) Landsat image False color composite image (NIR/Red/Green), (c) The damage region identified in this study (2010–2020), (d) damage region generated by GlobalLand30 (2010–2020), (g) damage region identified in this study (2010–2018), and (h–j) damage region generated by CLCD, NLCD, and MLC (2010–2018).

4.6. Defects of the Method and Future Work

In particular, the CCDC algorithm is suitable for surface mining disturbed identification, since the surface and related vegetation are damaged, while underground mining may have little impact on surface vegetation. The results may be affected by non-mining disturbances such as floods, and error sources need to be eliminated as much as possible [29].

Additionally, this study is a pixel-scale remote-sensing technology, which is difficult to avoid the phenomenon of “pepper and salt”, just as with previous studies [50,51]. In future work, we will preview and analyze the characteristics of spectral index trajectory changes on the GEE platform which can manage imageries and implement cloud computing [52,53]. Therefore, the algorithm can realize large-scale real-time monitoring of mining and reclamation. At present, China has issued laws and regulations such as The Regulations on Land Reclamation, which requires that people should reclaim what they destroyed, and mining while reclamation. This monitoring technology is urgently needed in the examination of reclamation projects, in sustainable mining management, and in regional eco-environmental impact assessment. In addition, this study also shows that the proportion of natural restoration and reclamation in the Dexing field is low, and it is necessary to further evaluate whether it can move towards sustainable mining. It just roughly measures the circumstances of mining disturbance with vegetation index singly, although it characterizes ground damage and vegetation restoration after mining. In the future, other parameters (such as terrain stability, resilience, erosion rate, etc.) should be integrated to ensure the environmental sustainability of mining production and the post-mining ecosystem.

5. Conclusions

In this study, we propose a new method to detect the continuous variation of disturbance in the mining area by processing Landsat time-series based on the GEE platform. Taking the largest copper mine in Asia as a research area, we firstly constructed a pixel-scale NDVI full-time series. Secondly, the CCDC algorithm is used for time segmentation, and the corresponding time segments of surface damage and reclamation in the mining field are obtained. This method can monitor the change of surface vegetation in mines.

The study shows that from 1986 to 2020, the surface mining area of Dexing Copper Mine continues to increase, with a cumulative damage area of 2865.96 ha and an average annual damage area of 81.88 ha. The whole damaged area shows a continuous fluctuation trend. Natural restoration and reclamation detection in the mining area had been 34 years from 1987 to 2020, and the total restoration area is 544.95 ha with an average annual recovery of 16.03 ha. The overall recovery area is less. From the perspective of the location in mining and restoration, the No. 1 and No. 2 tailing reservoirs have been restored after mining. The opencast field and No. 4 tailings reservoir in the mining area has continued to expand since 1986, and gradually transferred to the Fujiawu mining area after 2005. Vegetation restoration is concentrated in two phases: from 1994 to 1997, it centralized in No. 1 and No. 2 tailing reservoir, and mainly in the north side of No. 4 tailings reservoir, Xiyuan dump site and Tongchang mining area accompanied with the restoration efforts intensified after 2017. In addition, the detection also includes the change information, including the conversion year and month. After accuracy testing, the overall accuracy of damage and recovery is 92% and 88% respectively, and the Kappa coefficients are 85% and 84%, respectively. It can be found that the detection effect is ideal. Overall, the probability of land restoration after vegetation damage in our study area is low (19%). For the sustainable development of the mining area ecosystem, land managers should strengthen land reclamation and environmental management in mining areas.

The CCDC method of detecting continuous disturbed variation in mines based on Landsat time-series sequence and GEE platform has some characteristics including multi-segment splitting and higher sensitivity. It accurately identifies the time and times of surface disturbance in the mining area, and does well in efficiency and accuracy compared with other methods. It reduces human and financial resources in the detection of disturbance in mines. This method can be widely used in surface mining detection, so as to provide scientific and effective data for government and enterprises in the development and management, environmental governance, geological hazard monitoring, and ecological environment assessment of mines.

Author Contributions: M.Z. designed the whole research, and wrote the manuscript. T.H. performed the experiment and analyzed evaluation results. G.L., H.S. and D.L. took part in the conception of this study and checked the writing of the manuscript. W.X. and C.W. checked the writing of the manuscript. All authors have read and agreed to the published version of the manuscript.

Funding: This work was supported by the National Natural Science Foundation of China (72004197) and the National Key Research and Development Program of China (2016YFC0501103).

Data Availability Statement: Not applicable.

Conflicts of Interest: The authors declare that they have no known competing financial interests or personal relationships that could have appeared to influence the work reported in this paper.

References

1. Yi, K. Strategic thinking of high quality development of nonferrous metal industry in the new era. *China Nonferrous Met.* **2020**, *12*, 26–29.
2. Xiao, W.; Deng, X.; He, T.; Chen, W. Mapping Annual Land Disturbance and Reclamation in a Surface Coal Mining Region Using Google Earth Engine and the LandTrendr Algorithm: A Case Study of the Shengli Coalfield in Inner Mongolia, China. *Remote Sens.* **2020**, *12*, 1612. [[CrossRef](#)]
3. Li, J.; Jiang, Z.; Miao, H.; Liang, J.; Yang, Z.; Zhang, Y.; Ma, T. Identification of cultivated land change trajectory and analysis of its process characteristics using time-series Landsat images: A study in the overlapping areas of crop and mineral production in Yanzhou City, China. *Sci. Total Environ.* **2021**, *806*, 150318. [[CrossRef](#)]
4. Li, N.; Yan, C.Z.; Xie, J.L. Remote sensing monitoring recent rapid increase of coal mining activity of an important energy base in northern China, a case study of Mu Us Sandy Land. *Resour. Conserv. Recycl.* **2015**, *94*, 129–135. [[CrossRef](#)]
5. Bi, R.T.; Bai, Z.K.; Li, H.; Guo, Q.X. Spatiotemporal variation of land disturbance on Spatiotemporal variation of land disturbance on large opencast coal mine area. *Chin. J. Appl. Ecol.* **2007**, *18*, 1908–1912.
6. Nugroho, G.; Chulafak, G.A.; Yulianto, F. Rapid detection of land cover change in tropical savanna environment using conditional change vector analysis on remote sensing data in Moyo watershed, Sumbawa Regency, West Nusa Tenggara Province, Indonesia. *J. Degrad. Min. Lands Manag.* **2021**, *8*, 2731. [[CrossRef](#)]
7. Hua, W.; Qianpeng, Y.; Shanchuan, G.U.; Zeng, D.A.; Duoji, C. Monitoring on spatial-temporal vegetation dynamics based on Landsat time series. *Bull. Surv. Mapping.* **2020**, *11*, 7–12.
8. Arabameri, A.; Karimi-Sangchini, E.; Pal, S.C.; Saha, A.; Chowdhuri, I.; Lee, S.; Tien Bui, D. Novel credal decision tree-based ensemble approaches for predicting the landslide susceptibility. *Remote Sens.* **2020**, *12*, 3389. [[CrossRef](#)]
9. Sarp, G. Determination of vegetation change using thematic mapper imagery in Afşin-Elbistan Lignite Basin; SE Turkey. *Procedia Technol.* **2012**, *1*, 407–411. [[CrossRef](#)]
10. Townsend, P.A.; Helters, D.P.; Kingdon, C.C.; McNeil, B.E.; de Beurs, K.M.; Eshleman, K.N. Changes in the extent of surface mining and reclamation in the Central Appalachians detected using a 1976–2006 Landsat time series. *Remote Sens. Environ.* **2009**, *113*, 62–72. [[CrossRef](#)]
11. Hou, H.P.; Zhang, S.L.; Yan, Y.; Guo, S.Y.; Dun, D.G.; Jin, Y.J. RS and GIS Based Ecological Landscape Restoration in Xuzhou Northern Coal Mining Area. *J. China Univ. Min. Technol.* **2010**, *4*, 504–510.
12. Wu, C.; Du, P.; Tan, K. Analyzing land cover and landscape pattern change in coal mining area. *J. China Coal Soc.* **2012**, *37*, 1026–1033.
13. Fu, X. Monitoring of Vegetation Coverage Variation Based on Multi-Temporal Remote Sensing Data in Shendong Centre. *Environ. Monit. China* **2014**, *30*, 186–190.
14. Coops, N.C.; Hilker, T.; Bater, C.W.; Wulder, M.A.; Nielsen, S.E.; McDermid, G.; Stenhouse, G. Linking ground-based to satellite-derived phenological metrics in support of habitat assessment. *Remote Sens. Lett.* **2012**, *3*, 191–200. [[CrossRef](#)]
15. Wang, Y.; Li, X.; Li, F.; Wang, Y. Identification of typical disturbance trajectory in coal mining subsidence area based on multi-temporal remote sensing images. *Acta Geol. Sin.* **2019**, *93*, 301–309.
16. Li, J.; Jiao, L.P.; Shen, Y.Y.; Liu, Q.L. Land use and cover change in coal mining area by IFZ and NDVI. *J. China Coal Soc.* **2016**, *41*, 2822–2829.
17. Huang, C.; Goward, S.N.; Masek, J.G.; Thomas, N.; Zhu, Z.; Vogelmann, J.E. An automated approach for reconstructing recent forest disturbance history using dense Landsat time series stacks. *Remote Sens. Environ.* **2010**, *114*, 183–198. [[CrossRef](#)]
18. Verbesselt, J.; Hyndman, R.; Newnham, G.; Culvenor, D. Detecting trend and seasonal changes in satellite image time series. *Remote Sens. Environ.* **2010**, *114*, 106–115. [[CrossRef](#)]
19. Kong, Y.; Meng, Y.; Li, W.; Yue, A.; Yuan, Y. Satellite image time series decomposition based on EEMD. *Remote Sens.* **2015**, *7*, 15583–15604. [[CrossRef](#)]
20. Yin, Q.; Liu, C.; Tian, Y. Detecting dynamics of vegetation disturbance in forest natural reserve using Landsat imagery and Landtrendr algorithm: The case of Chaisong and Taibaishan Natural Reserves in Shaanxi China. *Acta Ecol. Sin.* **2020**, *40*, 7343–7352.

21. Brown, J.F.; Tollerud, H.J.; Barber, C.P.; Zhou, Q.; Dwyer, J.L.; Vogelmann, J.E.; Loveland, T.R.; Woodcock, C.E.; Stehman, S.V.; Zhu, Z. Lessons learned implementing an operational continuous United States national land change monitoring capability: The Land Change Monitoring, Assessment, and Projection (LCMAP) approach. *Remote Sens. Environ.* **2020**, *238*, 111356. [[CrossRef](#)]
22. Chai, B.; Seto, K.C. Conceptualizing and characterizing micro-urbanization: A new perspective applied to Africa. *Landsc. Urban Plan.* **2019**, *190*, 103595. [[CrossRef](#)]
23. Sulla-Menashe, D.; Friedl, M.A.; Woodcock, C.E. Sources of bias and variability in long-term Landsat time series over Canadian boreal forests. *Remote Sens. Environ.* **2016**, *177*, 206–219. [[CrossRef](#)]
24. Gorelick, N.; Hancher, M.; Dixon, M.; Ilyushchenko, S.; Thau, D.; Moore, R. Google Earth Engine: Planetary-scale geospatial analysis for everyone. *Remote Sens. Environ.* **2017**, *202*, 18–27. [[CrossRef](#)]
25. Kennedy, R.E.; Yang, Z.; Gorelick, N.; Braaten, J.; Cavalcante, L.; Cohen, W.B.; Healey, S. Implementation of the LandTrendr algorithm on google earth engine. *Remote Sens.* **2018**, *10*, 691. [[CrossRef](#)]
26. Yang, Y.; Erskine, P.D.; Lechner, A.M.; Mulligan, D.; Zhang, S.; Wang, Z. Detecting the dynamics of vegetation disturbance and recovery in surface mining area via Landsat imagery and LandTrendr algorithm. *J. Clean. Prod.* **2018**, *178*, 353–362. [[CrossRef](#)]
27. He, T.; Xiao, W.; Zhao, Y.; Chen, W.; Deng, X.; Zhang, J. Continues monitoring of subsidence water in mining area from the eastern plain in China from 1986 to 2018 using Landsat imagery and Google Earth Engine. *J. Clean. Prod.* **2021**, *279*, 123610. [[CrossRef](#)]
28. Liu, C.; Zhang, Q.; Luo, H.; Qi, S.; Tao, S.; Xu, H.; Yao, Y. An efficient approach to capture continuous impervious surface dynamics using spatial-temporal rules and dense Landsat time series stacks. *Remote Sens. Environ.* **2019**, *229*, 114–132. [[CrossRef](#)]
29. He, T.; Xiao, W.; Zhao, Y.; Deng, X.; Hu, Z. Identification of waterlogging in Eastern China induced by mining subsidence: A case study of Google Earth Engine time-series analysis applied to the Huainan coal field. *Remote Sens. Environ.* **2020**, *242*, 111742. [[CrossRef](#)]
30. Wang, H.; Xie, M.; Li, H.; Feng, Q.; Zhang, C.; Bai, Z. Monitoring ecosystem restoration of multiple surface coal mine sites in China via LANDSAT images using the Google Earth Engine. *Land Degrad. Dev.* **2021**, *32*, 2936–2950. [[CrossRef](#)]
31. Yu, Y.; Gan, F.; Zhou, P.; Han, Z. The dynamic monitoring of the exploitation environment based on CBERSE-02B satellite: A case study of the Dexing Copper Mine. *Remote Sens. Land Resour.* **2009**, *01*, 74–78.
32. Hansen, M.C.; Loveland, T.R. A review of large area monitoring of land cover change using Landsat data. *Remote Sens. Environ.* **2012**, *122*, 66–74. [[CrossRef](#)]
33. Karan, S.K.; Samadder, S.R.; Maiti, S.K. Assessment of the capability of remote sensing and GIS techniques for monitoring reclamation success in coal mine degraded lands. *J. Environ. Manag.* **2016**, *182*, 272–283. [[CrossRef](#)] [[PubMed](#)]
34. Meng, D.; Zhang, Z.; Feng, W. The Risk Analysis of Solid Waste of the Fujawu Copper Ore District Based on Goevee-1 and DEM. *Remote Sens. Land Resour.* **2011**, *02*, 130–134.
35. Liu, S.; Gan, F.; Wang, R. The application of hyperion data to extracting contamination information of vegetation in the dexing copper mine, Jiangxin Province, China. *Remote Sens. Land Resour.* **2004**, *59*, 7–10.
36. Loveland, T.R.; Dwyer, J.L. Landsat: Building a strong future. *Remote Sens. Environ.* **2012**, *122*, 22–29. [[CrossRef](#)]
37. Chen, S.; Woodcock, C.E.; Bullock, E.L.; Arévalo, P.; Torchinava, P.; Peng, S.; Olofsson, P. Monitoring temperate forest degradation on Google Earth Engine using Landsat time series analysis. *Remote Sens. Environ.* **2021**, *265*, 112648. [[CrossRef](#)]
38. Yin, H.; Prishchepov, A.V.; Kuemmerle, T.; Bleyhl, B.; Buchner, J.; Radeloff, V.C. Mapping agricultural land abandonment from spatial and temporal segmentation of Landsat time series. *Remote Sens. Environ.* **2018**, *210*, 12–24. [[CrossRef](#)]
39. Awty-Carroll, K.; Bunting, P.; Hardy, A.; Bell, G. Using Continuous Change Detection and Classification of Landsat Data to Investigate Long-Term Mangrove Dynamics in the Sundarbans Region. *Remote Sens.* **2019**, *11*, 2833. [[CrossRef](#)]
40. Zhou, Q.; Rover, J.; Brown, J.; Worstell, B.; Howard, D.; Wu, Z.; Gallant, A.L.; Rundquist, B.; Burke, M. Monitoring landscape dynamics in central us grasslands with harmonized Landsat-8 and Sentinel-2 time series data. *Remote Sens.* **2019**, *11*, 328. [[CrossRef](#)]
41. Zhu, Z.; Fu, Y.; Woodcock, C.E.; Olofsson, P.; Vogelmann, J.E.; Holden, C.; Wang, M.; Dai, S.; Yu, Y. Including land cover change in analysis of greenness trends using all available Landsat 5, 7, and 8 images: A case study from Guangzhou, China (2000–2014). *Remote Sens. Environ.* **2016**, *185*, 243–257. [[CrossRef](#)]
42. Barenblitt, A.; Payton, A.; Lagomasino, D.; Fatoyinbo, L.; Asare, K.; Aidoo, K.; Pigott, H.; Som, C.K.; Smeets, L.; Seidu, O. The large footprint of small-scale artisanal gold mining in Ghana. *Sci. Total Environ.* **2021**, *781*, 146644. [[CrossRef](#)]
43. Cohen, W.B.; Yang, Z.; Healey, S.P.; Kennedy, R.E.; Gorelick, N. A LandTrendr multispectral ensemble for forest disturbance detection. *Remote Sens. Environ.* **2018**, *205*, 131–140. [[CrossRef](#)]
44. Zhu, Z. Change detection using landsat time series: A review of frequencies, preprocessing, algorithms, and applications. *ISPRS J. Photogramm. Remote Sens.* **2017**, *130*, 370–384. [[CrossRef](#)]
45. Chen, J.; Cao, X.; Peng, S.; Ren, H. Analysis and Applications of GlobeLand30: A Review. *IJGI* **2017**, *6*, 230. [[CrossRef](#)]
46. Fang, C.; Wen, Z.; Li, L.; Du, J.; Liu, G.; Wang, X.; Song, K. Agricultural development and implication for wetlands sustainability: A case from Baoqing County, Northeast China. *Chin. Geogr. Sci.* **2019**, *29*, 231–244. [[CrossRef](#)]
47. Yang, J.; Huang, X. The 30 m annual land cover dataset and its dynamics in China from 1990 to 2019. *Earth Syst. Sci. Data* **2021**, *13*, 3907–3925. [[CrossRef](#)]
48. Zhang, H.K.; Roy, D.P. Using the 500 m MODIS land cover product to derive a consistent continental scale 30 m Landsat land cover classification. *Remote Sens. Environ.* **2017**, *197*, 15–34. [[CrossRef](#)]

49. Ma, X.; Tong, X.; Liu, S.; Luo, X.; Xie, H.; Li, C. Optimized sample selection in SVM classification by combining with DMSP-OLS, Landsat NDVI and GlobeLand30 products for extracting urban built-up areas. *Remote Sens.* **2017**, *9*, 236. [[CrossRef](#)]
50. Wei, L.; Wang, K.; Lu, Q.; Liang, Y.; Li, H.; Wang, Z.; Wang, R.; Cao, L. Crops Fine Classification in Airborne Hyperspectral Imagery Based on Multi-Feature Fusion and Deep Learning. *Remote Sens.* **2021**, *13*, 2917. [[CrossRef](#)]
51. Xiao, W.; Xu, S.; He, T. Mapping Paddy Rice with Sentinel-1/2 and Phenology-, Object-Based Algorithm—A Implementation in Hangjiahu Plain in China Using GEE Platform. *Remote Sens.* **2021**, *13*, 990. [[CrossRef](#)]
52. DeVries, B.; Huang, C.; Armston, J.; Huang, W.; Jones, J.W.; Lang, M.W. Rapid and robust monitoring of flood events using Sentinel-1 and Landsat data on the Google Earth Engine. *Remote Sens. Environ.* **2020**, *240*, 111664. [[CrossRef](#)]
53. Phalke, A.R.; Özdoğan, M.; Thenkabail, P.S.; Erickson, T.; Gorelick, N.; Yadav, K.; Congalton, R.G. Mapping croplands of Europe, Middle East, Russia, and Central Asia using Landsat 30-m data, machine learning algorithms and Google Earth Engine. *ISPRS J. Photogramm. Remote. Sens.* **2020**, *167*, 104–122. [[CrossRef](#)]